JOURNAL OF MATERIALS SCIENCE 30 (1995) 5002–5012

Nucleation and anisotropic crystalline growth of polyethylene under shear

B. MONASSE
Ecole Nationale Supérieure des Mines de Paris, Centre de Mise en Forme des Matériaux, Unité Associée au CNRS 1374, BP 207, 06904 Sophia Antipolis, France

The crystallization of polyethylene was observed during shear experiments in isothermal conditions. The nucleation and the crystalline growth rates were measured from a microscopic observation of the growing morphologies. An unusual formation and development of row nuclei was observed throughout the experiment, followed by anisotropic growth. Three main growth rates were measured with respect to the main directions of the process. All these growth rates are enhanced differently by the shear rate. This result is interpreted first by an increase of the equilibrium melting temperature emanating from an entropy loss due to the chain orientation, second the anisotropy of growth is discussed as an effect of chain orientation with respect to the growth front of lamellae and of a local flow different from macroscopic shear-flow. An overall kinetic equation with shear effect has been proposed for this polyethylene and tested in a stimulation of crystallization during injection moulding of a polyethylene disc. The shear effect on the crystallization is necessary to predict the crystallization temperature and the thickness of polymer crystallized during the filling stage.

1. Introduction

Thermal and mechanical conditions affect the crystallization mechanisms of polymers and the resulting kinetics. In industrial parts, such as injected parts, a multilayer structure is usually observed including complex morphologies as the result of thermal and mechanical conditions applied to the polymer melt. A large number of thermo-mechanical models seem to be able to predict the injection moulding process for the processing industry. Some of them describe mould filling as part of mould design systems, others describe structure development as a necessary link with polymer properties. Most of recent models include crystallization models in order to predict solidification. The data are obtained from crystallization experiments performed statically, with isothermal or constant cooling rate conditions. However, experiments under flow are necessary to test the validity of the crystallization models under flow, and to enable the prediction of crystallization in industrial processes with a computer-based model.

The effect of shear on crystallization kinetics has been described for polybutene-1 [1], polypropylene [2], poly ε-caprolactone [3], polyether-ether-ketone [4] and for various molecular weights of polyethylene [2, 5–10] and of polyoxyethylene [2, 3, 7, 11]. The results mainly concern the overall kinetics under shear of these polymers observed by dilatometry [3], viscosity [2, 4, 8, 10, 12] and birefringence [2, 8] measurements. Under isothermal conditions the overall kinetics is strongly increased by the shear effect with respect to static conditions [2, 3, 7, 13], which explains the reduction of induction time [2–4]. Shear during cooling consequently increases the crystallization temperature from the static condition [3]. A few experiments have shown the morphological development during shear flow [1, 14]. They exhibit two types of nuclei: randomly dispersed [1] and row nuclei [14]. The number of randomly dispersed nuclei increases with shear rate but without any effect on the shape and on the growth rate of spherulites [1–3]. Anisotropic morphologies formed from row nuclei were shown but without nucleation or growth rates measurements [14]. The morphologies observed after crystallization under shear are usually anisotropic in shape and oriented with respect to the shear direction [4, 10, 13–15]. In spite of these anisotropic morphologies usually observed after shear-induced crystallizations, few experiments have been devoted to the analysis of nucleation, growth and morphology development during shear [1, 2].

Previously, the morphological and kinetic behaviours were not directly coupled. The main aim of the present work was to measure nucleation and growth rates from direct morphological observations of a polyethylene under shear. These results were then analysed according to models under flow, and transformed to obtain an overall kinetics under shear. This overall kinetics model has been applied in a computer program of injection moulding [16] to predict the crystallization behaviour. The predictions of the program with and without shear effect in the overall kinetics are compared with morphologies observed after injection moulding experiments.

0022–2461

2. Experimental procedure

2.1. Shear apparatus

Under static conditions, the isotropic growth rate of spherulites is strongly dependent on crystallization temperature. Its measurement is usually performed by optical microscopy in a hot stage under isothermal conditions. A hot stage with low thermal lag is necessary to reach isothermal conditions quickly and avoid crystallization during the cooling period. A high precision of temperature control is necessary to maintain a constant temperature throughout the crystallization process. Several commercial devices are available for this application. These thermal characteristics are also required for crystallization experiments under shear and isothermal conditions. The shear is applied to the polymer melt by the relative movement of two parallel plates separated by a constant distance, e. A special device was designed to observe morphologies during isothermal crystallizations under shear conditions (Fig. 1). The apparatus was designed to impose a constant longitudinal speed, V_x, from which the mean shear rate, $\dot{\gamma}$, is calculated from

$$\dot{\gamma} = \frac{dV_x(z)}{dz} = \frac{V_x}{e} \quad (1)$$

The second equality of Equation 1 assumes that the shear rate is constant through the thickness. The polymer is observed by optical microscopy with light transmission through two parallel glass plates. The molten polymer is maintained by these plates, $e = 70$ μm apart. They are shaped as glass rails oriented in the longitudinal direction. The width of the rails is $l = 2$ mm and their thickness 300 μm, in order to locate the shear only between the rails. The length of the rails allows a 40 mm translation. This geometry controls the contact between the glass plates and the polymer, and allows the observation of the crystalline morphologies over the width of the glass rails. Each of them is heated by an aluminium hot plate. The hot plates are parts of a Mettler FP 52 hot stage with a platinum 100 Ω temperature gauge inserted. The upper glass rail and aluminium hot plate are fixed in position. The position and the longitudinal displacement of the lower glass rail are controlled by two guide rails. A constant speed along this direction is induced by a d.c. motor through a screw–thread system. Then a rectangular hole was machined in the lower aluminium plate in order to observe the polymer throughout the experiment (Fig. 1). A stress gauge measures the shear stress during the experiment. A higher thermal stability was obtained by a constant nitrogen flux which regulates the heat loss from the hot stage and reduces polymer oxidation. This apparatus is able to heat the polymer from room temperature to $T = 300$°C with a 0.1°C accuracy. The cooling can be controlled with a 8°C min^{-1} maximal cooling rate down to $T = 100$°C.

The temperature of this hot stage is controlled by a Mettler FP 5 controller module. The temperature in the sheared zone was calibrated under static conditions with standards of thermometry (benzoic acid $T_m = 122.35$°C; anisic acid $T_m = 183$°C). This calibration leads to an 0.1°C temperature accuracy. With this geometry, the shear rate, $\dot{\gamma}$, is only defined by the longitudinal speed of the lower plate. The maximum speed, $V_{x\,max} = 300$ μm s^{-1} leads to a maximum shear rate $\dot{\gamma} = 4.2$ s^{-1}. The thickness of the sheared films was checked after crystallization.

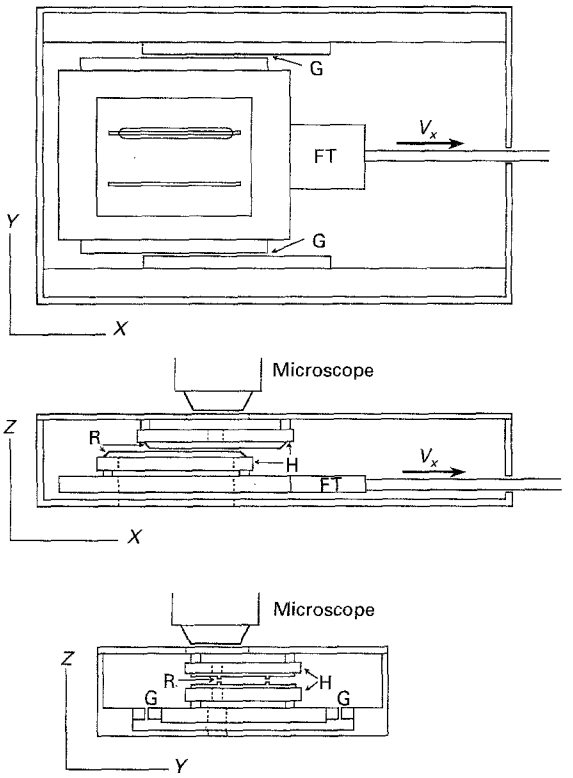

Figure 1 Shear apparatus; G, guide rails; R, glass rails; H, hot plates; FT, force transducer.

2.2. Material and experimental procedure

A linear medium density polyethylene was supplied by Norsolor under reference MG 2210. Its density ($\rho = 940.4$ kg m^{-3}) results from a copolymerization of ethylene (molar content by 1000 carbons: 482.6) with butene-1 (7.3 mol‰/C) and isobutene (1.4 mol‰/C) which leads to 7.3‰ C_2H_5/carbon and 10.1‰ CH_3/carbon. The molecular weight was measured by GPC: $\bar{M}_n = 17\,000$; $\bar{M}_w = 64\,000$; $\bar{M}_z = 170\,000$.

Polymer films (thickness 150–200 μm, width 2 cm, length 5 cm) were prepared by melting pellets between two glass slides and then solidifying them by air cooling down to room temperature. Polymer sections, 5 cm long and 5 mm wide, were cut from these films and inserted between the spaced glass rails at room temperature. Then the sample was slightly pressed during the closing of the apparatus at room temperature. The polymer film was melted by the glass rails to $T = 150$°C and pressed to its final thickness ($e = 70$ μm). The film thickness was fixed by the spacers. This procedure reduced the initial deformation of the polymer film and fixed a sample reference state before shear experiments. The apparatus was set under the microscope and cooled without shearing down

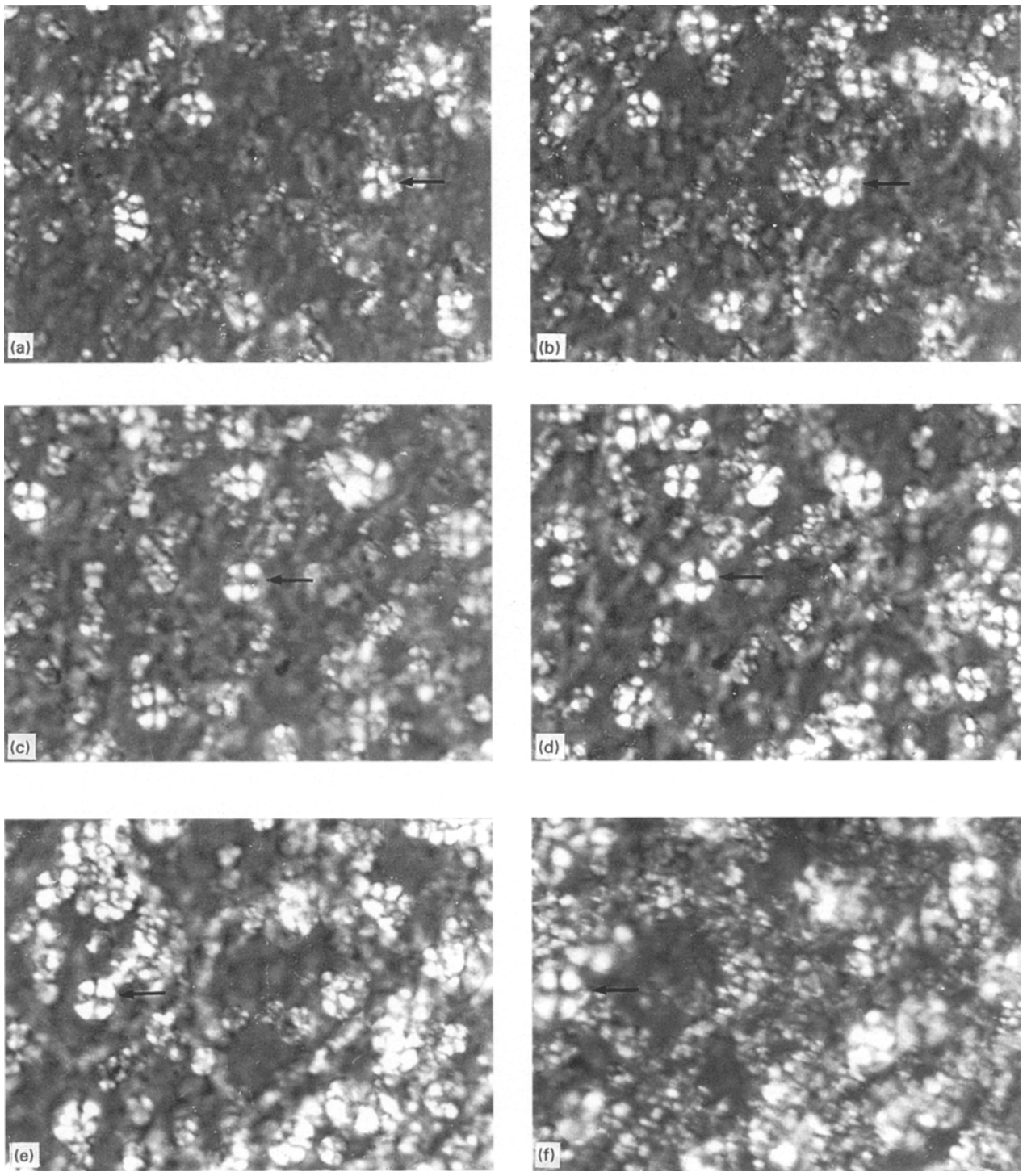

Figure 2 Successive morphologies observed during a shear experiment ($T_c = 117°C$, $\dot{\gamma} = 2.6\,s^{-1}$) along the direction of movement; the arrows indicate a particular morphology. (Scale = 40 μm)

to the crystallization temperature $T_c = 117°C$. A constant shear was applied when isothermal conditions, were reached. Under these thermal conditions, no crystallization was observed before the beginning of shear. The effective observation of morphologies and the measurement of the shear force then began. The experiment was performed until the sample broke after about the half-transformed volume fraction ($\alpha = 0.5$). Micrographs of the morphologies were taken at constant time intervals through a Reichert Zetopan-Pol microscope under polarized light. During shear experiments the morphologies pass through the observation window fixed by the microscope during a period shorter than the crystallization time. In order to increase the precision of the growth rate measurement, the radius versus time curve was reconstructed from successive morphologies observed at different periods. An overlapping of at least two successive morphologies on a micrograph was considered during each experiment (Fig. 2). Consequently, each kinetics data is a composite result obtained from an overlapping of data from various morphologies. By this way it is possible to extend the period for the analysis of crystal growth and to obtain some

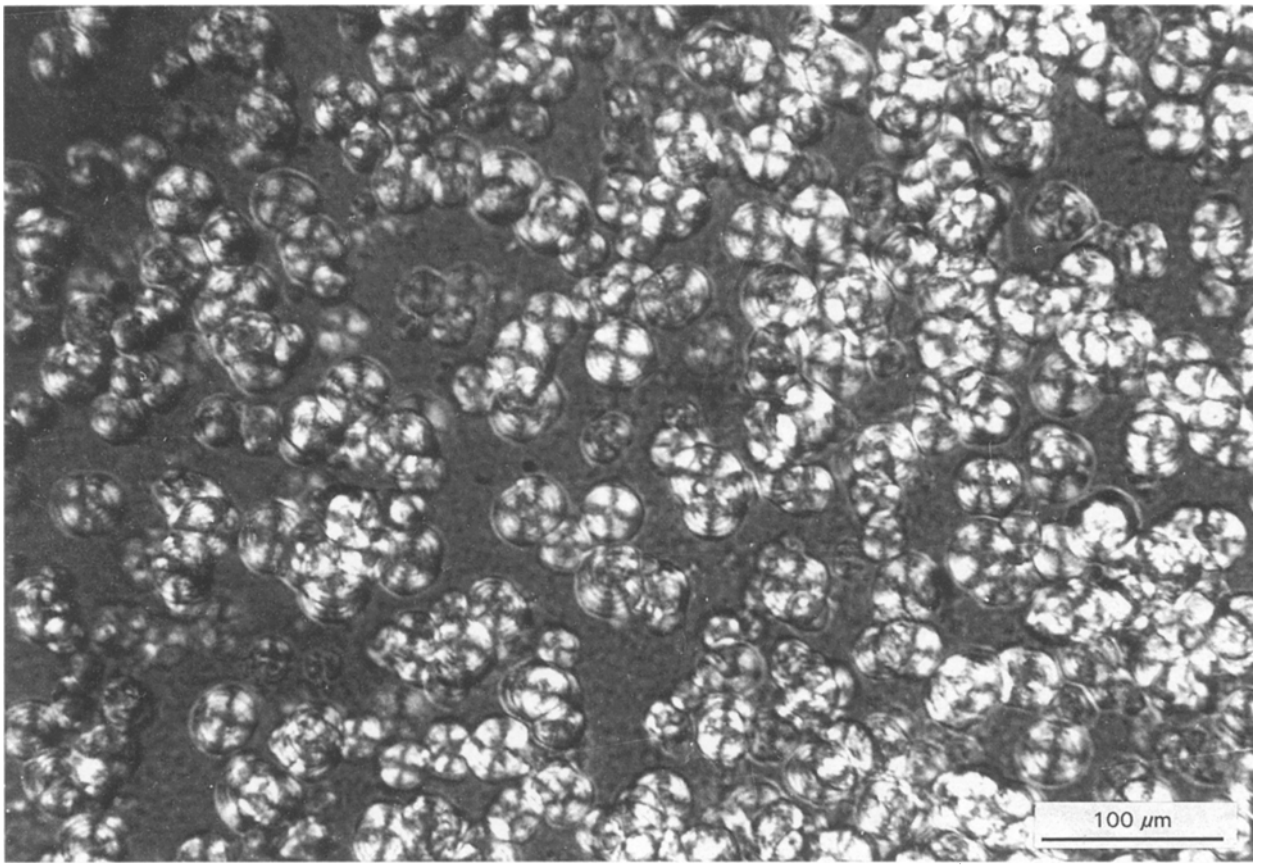

Figure 3 Spherulites observed under static conditions ($T_c = 117°C$).

indication on activated nuclei. The size difference of morphologies at the same time indicates a difference in the activation time, assuming a constant growth rate in time as discussed below.

Throughout the analysis of experimental results, three main directions were considered according to the geometry of the machine (Fig. 1): longitudinal, i.e. parallel, to the movement (X), through the sample thickness (Z), and the direction perpendicular to the previous ones (Y). Thin sections, 5 μm thick, were cut out of solid sheared samples with an ultramicrotome LKB Ultrotome II equipped with a glass knife. These thin sections cut in the shear plane (XZ) and perpendicular to the shear direction (YZ) were observed by optical microscopy between glass plates in an immersion oil to detect any possible three-dimensional anisotropy.

3. Results

The experiments were performed at 117°C under five shear rates ($\dot{\gamma} = 1.15, 2.2, 2.6, 3.05$ and $4.2\ s^{-1}$), and statically. At least two experiments were performed for each condition.

3.1. Nucleation under shear

A static experiment without any shear was performed as a reference. The activated nuclei seem to be randomly distributed in the plane of observation (XY) (Fig. 3). The spherulites growing from these nuclei are ringed and isotropic in shape. The spherulite growth can be defined by one growth rate which is constant throughout the experiments: $G = 0.22\ \mu m\ s^{-1}$.

Nucleation and growth rate are significantly different when a shear is applied during crystallization. During the first stage of crystallization the morphologies appear aligned along the Y direction (Fig. 4a). This row nucleation appears in the transverse direction with respect to the plate movement (X), i.e. perpendicular to the direction usually observed after crystallization [1]. The relative position of these nuclei as revealed by the subsequent morphologies changes during shear experiments (Fig. 4b–d). A cell organization appears from the initial row nuclei. Some of these initial nuclei turn from the Y direction to the X direction, other nuclei seeming unchanged in orientation (Fig. 4b–d). This process of row nucleation and of change in orientation appeared during all shear experiments but not in the static test. Consequently, this nucleation process is specific to shear experiments. The possibility of an artefact arising from the preparation of the sample must be rejected, because the same procedure was used for all the experiments, including the static experiment which exhibits a random nucleation. A previous shear can act on subsequent nucleation [17] and may appear during the pressing of molten polyethylene to the final thickness. This hypothesis could explain the transverse nucleation (Y direction), but must be rejected in view of the usual random nucleation during static experiments. This row nucleation and the cell formation have not been

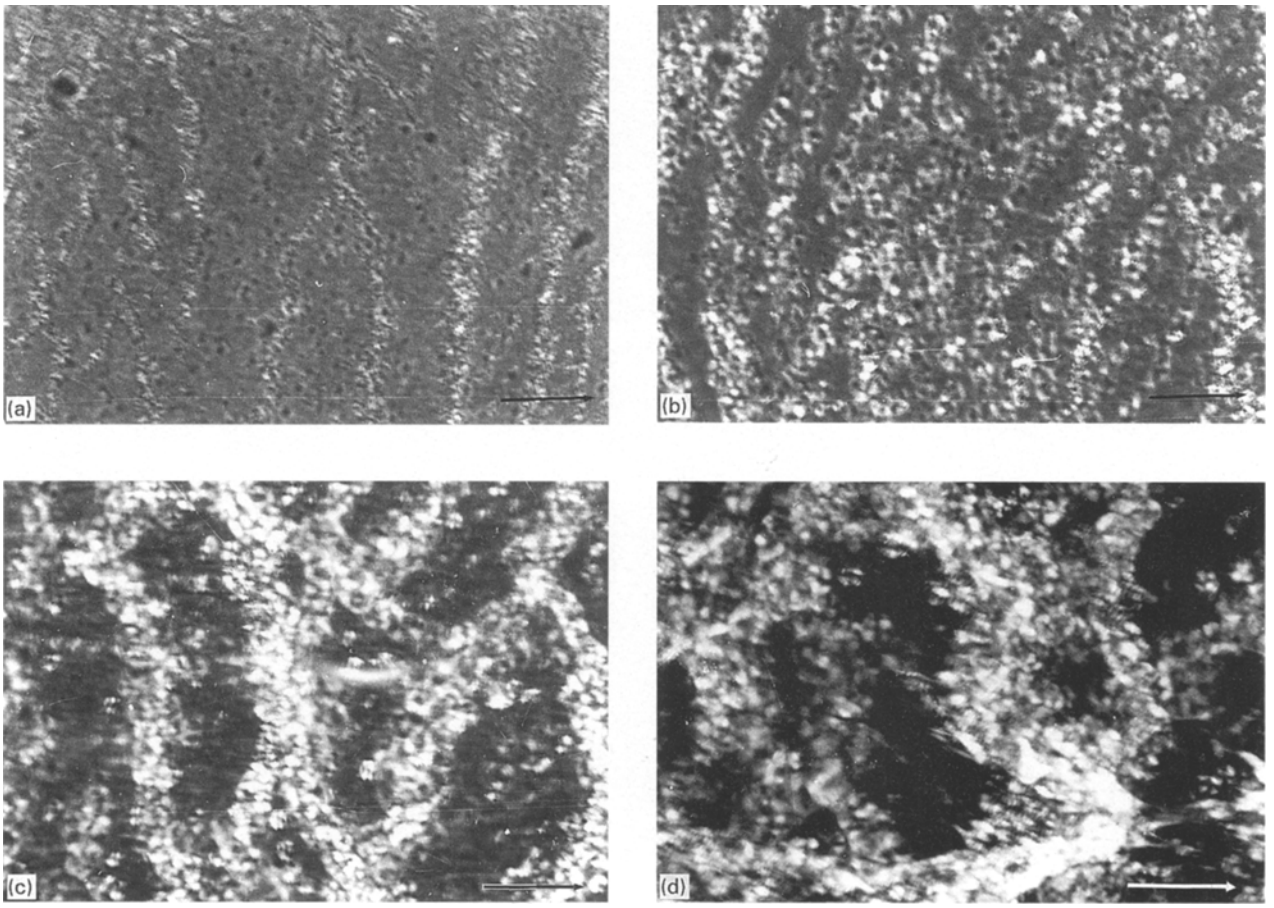

Figure 4 Transverse row nucleation and cellular organization observed during a shear experiment ($T_c = 117°C$, $\dot{\gamma} = 4.2\,s^{-1}$), the arrow indicates the direction of movement. (Scale = 150 μm)

previously described and are not explained at the moment.

3.2. Anisotropic morphologies under shear

Nucleation is revealed by the subsequent crystalline morphologies which grow separately from each of these activated nuclei. The morphologies are observed in the XY plane during static and shear experiments. The shape of each of these morphologies can be analysed independently of the others during shear experiments. At any stage of the growth, the morphologies are always elliptical in shape during shear whereas spherulites appear only as circles during static crystallization. All these ellipses have the same orientation which is maintained throughout the experiment. The long axis of the ellipses ($2r_y$) is along the transverse direction (Y) and the short axis ($2r_x$) along the translation direction (X). These main directions seem unmodified during the shear experiment. The shape ratio, r_y/r_x does not change during a shear experiment. The shear rate, $\dot{\gamma}$, seems to be the only factor which alters the shape ratio r_y/r_x (Fig. 5). Increasing shear rate increases the shape ratio. This anisotropy in shape persists up to the junction with neighbouring morphologies.

In these experiments the shear plane is XZ and not the observed XY plane. In order to observe morphologies along the shear plane, microtomed sections,

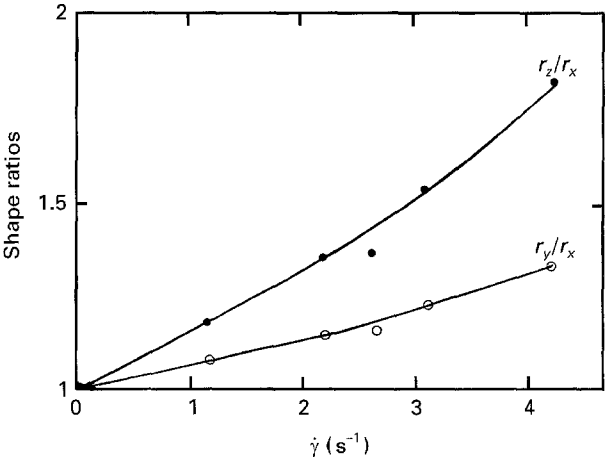

Figure 5 Shape ratio of the radii r_y/r_x and r_z/r_x as a function of shear rate.

5 μm thick, were cut off in the XZ plane after crystallization (Fig. 6). The morphologies have a higher extent along the sample thickness (Z direction). Concentric rings with elliptical shape are always observed inside the morphologies. These rings are a clear indicator of the shape of each morphology. During isothermal crystallizations under static conditions this ring spacing is constant along the radius and the rings are concentric up to the limit of the growing spherulites [3]. They are usually interpreted as a cooperative

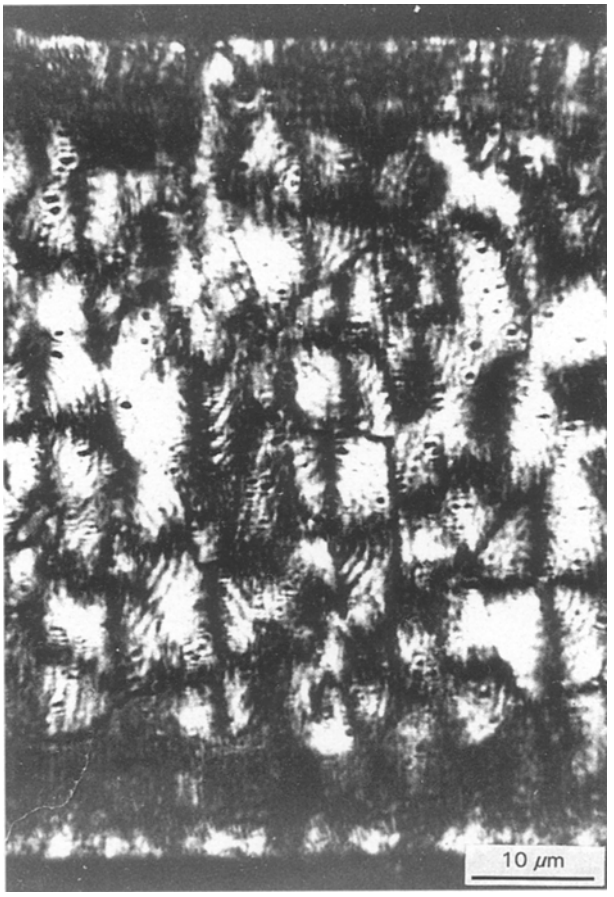

Figure 6 Ringed morphologies observed in the shear plane $XZ(T_c = 117°\,C, \dot{\gamma} = 4.2\,s^{-1})$.

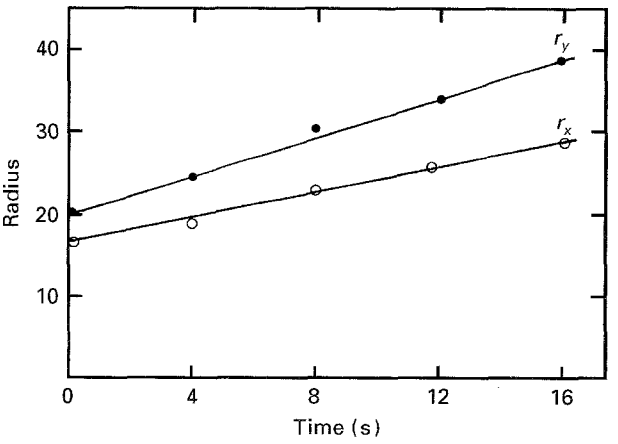

Figure 7 Growth rate measurements, G_y and G_x, deduced from the radius measurements r_y and r_x as a function of time, respectively $(T_c = 117°\,C, \dot{\gamma} = 4.2\,s^{-1})$.

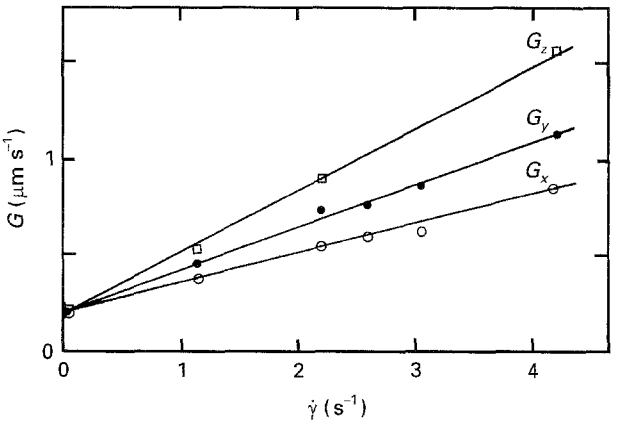

Figure 8 Growth rate measurements of G_x, G_y and G_z as a function of shear rate.

twisting of polyethylene lamellae [4]. The non-constant spacings observed in our experiments are artefacts arising from a random intersection of a plane with a sphere. This spacing is constant along a direction when the thin polymer slice includes the centre of the morphology, i.e. its nucleus. Measurements are restricted to those morphologies with a constant spacing along a radius exhibiting the lowest spacing value. This is the reason why we associate the ring spacing anisotropy with the shape of the growing morphologies. So, the ring anisotropy of the final morphologies is used to calculate the size anisotropy, r_z/r_x, which cannot be observed during crystallization, because Z is the direction of observation under shear. The two shape ratios, r_y/r_x and r_z/r_x systematically increase with the shear rate (Fig. 5). The highest morphological extension is along the Z direction. Analysis of growth rates is now the key point for the understanding of this morphological anisotropy.

3.3. Anisotropy of crystalline growth under shear

Under static conditions, whatever the direction, the radial growth of this polyethylene is isotropic: $G = 0.22\,\mu m\,s^{-1}$ at $T_c = 117°\,C$. This value is usual for a medium density polyethylene [5] and results from an isotropic growth of radial lamellae at the same speed. The growth rates were measured under shear with the procedure described in Section 2.2. The growth along the direction of observation (Z direction) is not observed. In the XY plane, the morphologies exhibit no change of the shape ratio during their growth. The morphological anisotropy results from the anisotropy of the growth kinetics and the growth rate measurements can be reduced to the knowledge of the growth rate along the two main directions of the apparatus (Fig. 4).

In the XY plane, the two main growth rates are constant with time, as observed under static conditions (Fig. 7). This effect reveals that the crystal growth rates are controlled by an interfacial process. Basically in this range of shear rate this interfacial process is assumed to be identical under static and under shear conditions; only the rate constants change (Fig. 8). The growth rates, G_x and G_y, increase with the shear rate from the static condition. The main effect of shear rate is to increase the growth rate and to produce an anisotropy of crystalline growth. The growth rate anisotropy can be reduced to the main growth rate directions. The main directions of growth coincide with the main-shape directions and with the apparatus main directions. The growth rate anisotropy, G_y/G_x, and the morphological anisotropy, r_y/r_x, are found to be equal in all experiments (Figs 5 and 8). A possible anisotropy of initial morphologies does not affect the adequacy of anisotropies of growth rate and

of growing morphologies, as observed under static conditions. Consequently, the anisotropies of growth rate and of morphology will be superimposed and used indiscriminately. This conclusion, obtained for the anisotropy analysis in the plane XY, has been applied to the anisotropy in the plane XZ measured on thin cuts after crystallization (Fig. 8).

All the three main growth rates strongly increase with shear rate from the static condition (index 0): $G_{z(4.2\,s^{-1})} > 6G_{z0}$ and $G_{x(4.2\,s^{-1})} > 3G_{x0}$. The growth rates seem to increase linearly with the shear rate. The slope depends on the direction: $dG_z/d\dot{\gamma} = 0.32\ \mu m$, $dG_y/d\dot{\gamma} = 0.225\ \mu m$, $dG_x/d\dot{\gamma} = 0.16\ \mu m$. It is necessary to analyse these results with existing theories of crystallization under flow. No theory seems able to explain, at the same time, the increase of all three main growth rates and the resulting anisotropies of growth.

3.4. Analysis of enhancement of crystalline growth

The increase of the three growth rates results from the shear flow effect. The shear flow deforms the polymer chain from the random coil, reduces the number of possible conformations of the chains and the entropy S, of the polymer melt. The equilibrium melting temperature, T_m^0, is defined by

$$\Delta G_{(T_m^\circ)} = \Delta H - T_m^0 \Delta S = 0 \quad (2)$$

where ΔG is the free energy, ΔH and ΔS the enthalpy and entropy of crystallization (or fusion), respectively. If we consider that ΔH is not affected by the polymer flow, the equilibrium melting temperature, T_m^0, must increase as a result of entropy reduction [18–22]

$$T^\circ_{m(\dot{\gamma})} = \frac{\Delta H}{\Delta S_{(\dot{\gamma})}} \quad (3)$$

Under static conditions the crystalline growth rate of a polymer depends only on undercooling $\Delta T = T_m^\circ - T_c$, where T_c is the crystallization temperature. The growth rates under shear and static conditions are time constant. This result implies that the growth rate is controlled by an interfacial process under stationary conditions. If a transient period exists it must appear within the first seconds under shear as well as during static conditions. This possible transient period is not revealed by the present experiments. The interfacial process concerns the deposit of polymer segments from the melt on the growth front of the crystalline lamellae. This deposition process basically appears unmodified by the shear flow in the present range of shear rates. The entropy loss seems to be the main parameter which controls the increase of growth rates by an increase of the equilibrium melting temperature. If we assume that only undercooling, ΔT, acts on the growth rate it is possible to calculate the increase of T_m° under shear. Then we consider the equality of growth rate under static conditions, $G_o(T_c)$, with the mean growth rate, $G_s(T_c')$, observed under shear for the same undercooling

$$G_o(T_c) = G_s(T_c') = [G_x(T_c')\,G_y(T_c')\,G_z(T_c')]^{1/3} \quad (4)$$

It is necessary to know the effect of crystallization temperature on growth rate under static conditions to deduce $T_m^0 = f(\dot{\gamma})$. A linear function, $T_m^0(\dot{\gamma}) = A\dot{\gamma} + T_m^0$, seems able to describe our results, with $A = 0.6^\circ$ Cs. The derivation from $\dot{\gamma}$ of Equation 3, including this relationship, implies that $d(\Delta S)/d\dot{\gamma} = 2.79 \times 10^{-2}\ J\,s\,mol^{-1}K^{-1}$, with $\Delta S = 19.4\ J\,mol^{-1}K^{-1}$ ($\Delta H = 290\ J\,g^{-1}$ $T_m^0 = 418$ K) [23]. This increase of T_m^0 can be compared with a similar prediction deduced from the analysis of induction time performed on a polyethylene [24]. This variation is attributed to a change in the nucleation rate and not in the growth rate. Nevertheless, in the same range of shear rate (up to $9\ s^{-1}$) the slopes are almost the same ($A = 0.3 - 0.7^\circ$Cs) as the value we found ($A = 0.6^\circ$ Cs). As an effect of this variation of T_m^0, the same order of magnitude is found for entropy variation with shear rate $d(\Delta S)/d\dot{\gamma} = 3.29 \times 10^{-2}\ J\,s\,mol^{-1}K^{-1}$.

3.5. Anisotropy of crystalline growth

The anisotropy of crystalline growth is not explained by this thermodynamic model which is basically isotropic. Nevertheless, a crude model predicts an increase of the mean extension of the chain along the directions $X > Y > Z$ and a more and more favourable parallel orientation of the chain with respect to the nucleation surface (NS) along $NS_x < NS_y < NS_z$. Consequently, the growth rate must be enhanced for the transverse orientation of lamellae with respect to oriented chains, G_z, rather than in the chain orientation, $G_x.G_y$ is in an intermediate situation. Effectively we observe for any shear rate, $G_z > G_y > G_x$ (Fig. 8). This crude description is not able to predict the apparent linear increase of the growth rates with the shear rate in the range $0\ s^{-1} \leq \dot{\gamma} \leq 4.2\ s^{-1}$. The development of this growth rate anisotropy explains the morphological anisotropy as observed after crystallization under shear. This effect seems to be connected with the nucleation event: the row nuclei link the growing morphologies and prevent the rotational contribution of shear flow for individual morphologies. The fixing of the orientation of the morphology is necessary to maintain the growth rate anisotropy. A macroscopic shear-flow is applied in the experiment but a local extensional flow must appear in the neighbourhood of growing morphologies as an effect of blocking the rotational contribution. Consequently, the morphology could develop from the local flow and not from the macroscopic experiment. This analysis implies a strong connection between row nucleation and the growth anisotropy associated with a strong increase of the growth rate. This result is consistent with our observations on events of row nucleation and of growth rate anisotropy. Previous analyses exhibit neither specific row nucleation nor anisotropic growth of increase of growth rate under shear [1, 2].

TABLE I Experimental conditions for injection moulding

Sample	Injection rate ($cm^3 s^{-1}$)	Injection temperature (°C)	Mould temperature (°C)
Low rate	50	220	25
High rate	200	220	25

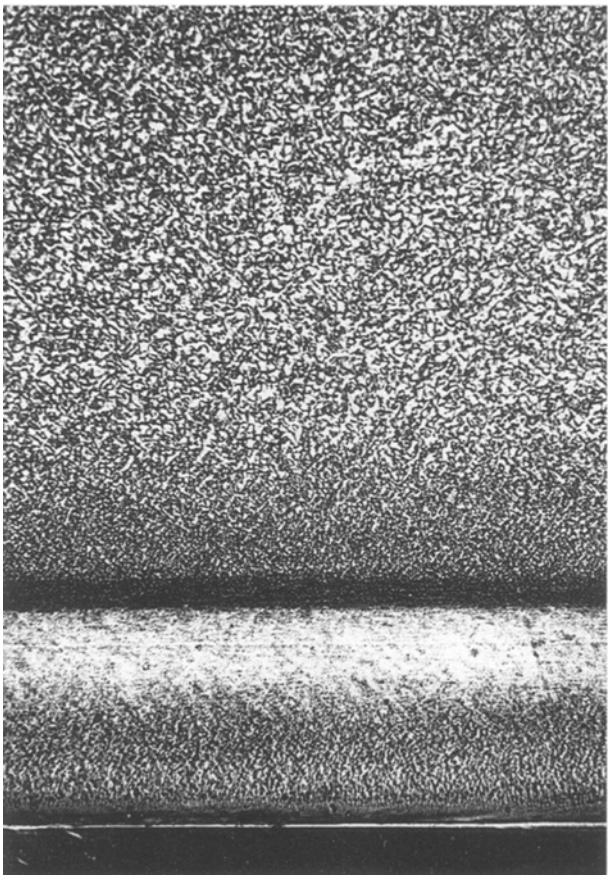

Figure 9 Layers observed in the thickness of a disc, 2 mm thick. Thickness of the cut = 10 μm. Radius = 100 mm from the central gate; $\dot{V} = 50\ cm^3 s^{-1}$. (Scale = 100 μm)

3.6. Prediction of the overall kinetics under shear

The overall kinetics including the effects of shear rate is deduced from these and static experiments. The results were analysed according to Ozawa's model under constant cooling rate [25], here defined as (St)

$$\alpha(T, \dot{T}) = 1 - e^{-E(T,\dot{T})} \quad (5)$$

$$E(T, \dot{T}) = \frac{\chi(T)}{\dot{T}^n} \quad (6)$$

where α is the conversion of a semi-crystalline polymer from the melt, $\chi(T)$ is the rate constant and n is the Avrami exponent. Under static conditions, $\chi(T)$ depends on nucleation rate, growth rate and growth geometry of crystalline morphologies (only a function of crystallization temperature). $\chi(T)$ and n are deduced from polyethylene data under static conditions analysed according to Equation 7

$$\ln\{-\ln[1 - \alpha(T, \dot{T})]\} = -n \ln \dot{T} + \ln \chi(T) \quad (7)$$

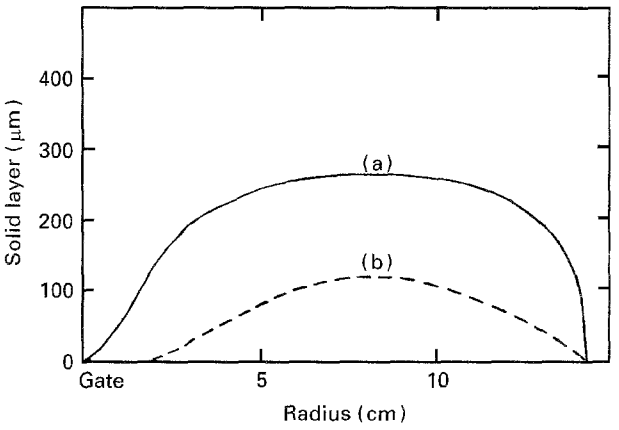

Figure 10 Calculated thickness of the layer crystallized during the filling stage along the radius under two different flow rates; (a) $\dot{V} = 50\ cm^3 s^{-1}$, (b) $\dot{V} = 200\ cm^3 s^{-1}$.

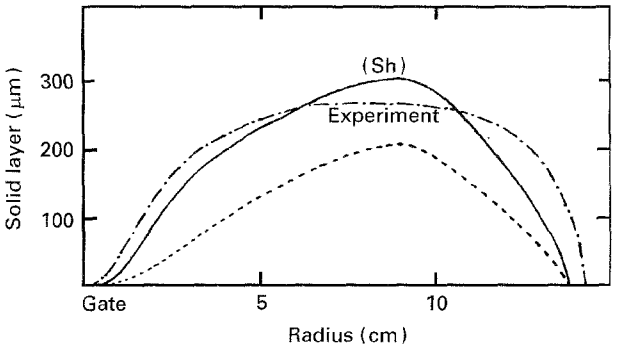

Figure 11 Thickness of the layer crystallized during the filling stage compared with the predictions of the thermo-mechanical models, including the crystallization kinetics with (Sh) and without (St) shear effect; $\dot{V} = 50\ cm^3 s^{-1}$.

The Avrami exponent $n = 3$ is analysed as an initial nucleation followed by spherulitic growth. This result is deduced from microscopic observations of static crystallization under isothermal conditions (Fig. 3). Consequently, $\chi(T)$ can be expressed as

$$\chi(T) = \frac{4}{3}\pi N_0 G_0^3(T) \quad (8)$$

Papers indicate an increase of the Avrami exponent well above $n = 4$ for crystallization under shear [6, 13], while some experiments describe a decrease of n down to $n = 2$ [26]. These values were deduced from overall experiments without direct observation during crystallization. From the present observations we prefer to consider the anisotropy of growth rather than the nucleation effect. From this point of view an increase of shear rate enhances the growth anisotropy and leads to a two-dimensional growth. We have shown that the growth is still controlled by an interfacial process. Therefore, this reduction of growth dimension promotes at the most a one-unity decrease of the Avrami exponent, from 3 to 2. The shear rate mainly modifies the growth rates of this polyethylene and therefore the overall kinetics. Ozawa's model is considered to be still valid with an extension coming from the shear effect, here defined as (Sh)

$$\alpha = 1 - e^{-E(T,\dot{T},\dot{\gamma})} \quad (9)$$

with the mathematical expectancy $E(T, \dot{T}, \dot{\gamma})$

$$E_{T,\dot{T},\dot{\gamma}} = \frac{4}{3}\frac{\pi N_0 (1 + 3.075\,\dot{\gamma})^3 G_0^3}{\dot{T}^{\left(2+\frac{1}{1+0.2\dot{\gamma}}\right)}} \quad (10)$$

A reduction of the Avrami exponent from 3 to 2 is described from static conditions to high shear rate $\dot{\gamma} > 20\,s^{-1}$ [26]. This effect can be explained by an increase of row nucleation which here allows only a two-dimensional growth ($n = 2$). The growth rate increase is only considered in this equation and the nucleation is assumed to be unmodified. The large increase of the growth rate is quantified while the change in the density of nuclei seems to be lower. For example, with $\dot{\gamma} = 4.2\,s^{-1}$, the factor $G_z G_y G_x = 140\,G_0^3$ (G_0 is the static growth rate) while N_0 does not increase so much. The parameter $G_z(\dot{\gamma})\,G_y(\dot{\gamma})\,G_x(\dot{\gamma})$ takes the place of G_0^3 as the form $G_{z(\dot{\gamma})}\,G_{y(\dot{\gamma})}\,G_{x(\dot{\gamma})} = (1 + 3.075\dot{\gamma})^3\,G_0^3$. The mathematical expectancy can be expressed in a form compatible with the conversion rate deduced from isothermal experiments. The shear rate acts both on $\chi(T, \dot{\gamma})$ and on the Avrami exponent $n(\dot{\gamma})$. Consequently, this model is able to predict a morphological change.

3.7. Prediction of crystallization during the filling stage of injection moulding of a disc

This overall crystallization kinetics law, Equations 9 and 10, is now implemented into a thermo-mechanical model of injection moulding [16, 27, 28]. This model here must describe the thermal and mechanical conditions during the filling stage inside a disc injected from a central gate [16, 27, 28]. The thermal, mechanical and crystallization effects are strongly coupled. The first link comes from the crystallization. It is a cumulative phenomenon which must take into account the thermal (temperature and cooling rate) and mechanical past history which acts on each particle. The second link comes from the change of boundary condition (velocity = 0) which moves from the surface of the mould to the interface between the solid and still molten polymer. This interface is defined by the polymer crystallization, then the velocity field and therefore the shear rate are enhanced inside the still molten polymer. The third link comes from the heat of crystallization which must be taken into account in the energy equation. These links are implemented in the computer program.

The predictions of the model are specifically tested for the filling stage of the injection moulding process with conditions defined in Table I. The thickness of the polymer layer and the crystallization temperature of the inner morphology, solidified during this period, are measured to test the predictions of the model. These experimental results are compared with the corresponding thicknesses of the solid layer at the end of the filling stage, and the crystallization temperatures calculated with two forms of the crystallization kinetics: a thermal and shear dependent kinetics (Sh) (Equations 9 and 10), and a purely temperature dependent kinetics (St) (Equations 5 and 6). This comparison must demonstrate the importance of the shear effect on the crystallization behaviour and the ability of such a model to predict polymer solidification during the injection moulding process.

The polymer crystallizes under a high cooling rate and under rapid flow, mainly shear effect, during the filling stage. On the contrary, during the packing–cooling stage, a lower flow is applied to the crystallizing polymer. The oriented morphologies crystallized under flow, mainly under shear flow, are clearly different from the spherulites formed under quasi-static conditions. This fact is applied to define the limit of the layers which are crystallized during the filling stage from each surface of the mould device. This limit is measured along the radius on a thin section, 10 μm thick, cut out in the thickness of the discs by polishing (Fig. 9). The thickness of the solid layers formed during the filling stage can be measured with a ± 10 μm accuracy along the radius of the injected part (Fig. 9). Except near the central gate, the layers are identical on both sides whatever the location along the radius or the injection condition. Consequently, half of the thickness will be considered for the morphological description and the stimulation. The thickness of this layer is strongly enhanced by a decrease of the injection rate (Fig. 10). This thickness can be calculated by the thermo-mechanical model using a crystallization model with (Sh) and without (St) shear effect (Fig. 11). The crystallization model (Sh) predicts correctly the shape and the thickness of the solid layer, whereas this thickness is underestimated by the model (St). This underestimate is very large, about 50% of the thickness, for the higher injection rate. The shear rate and its effect are more important in this condition than for the lower injection rate.

This change in the thickness must result from an increase of the crystallization kinetics and therefore of the crystallization temperature. The morphologies were analysed in order to measure the local crystallization temperature through the thickness of the injected parts. Under static conditions, the ring spacing of these spherulites depends on the crystallization temperature. For each crystallization temperature, this spacing is measured during isothermal experiments (Fig. 12). The thin cuts of the injected parts are now

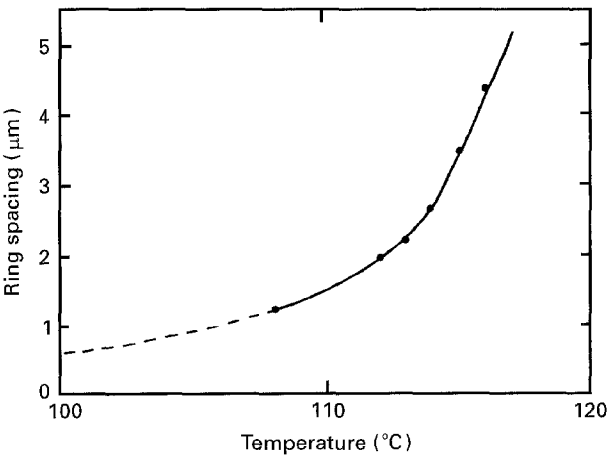

Figure 12 Ring spacing of the spherulites crystallized under isothermal conditions.

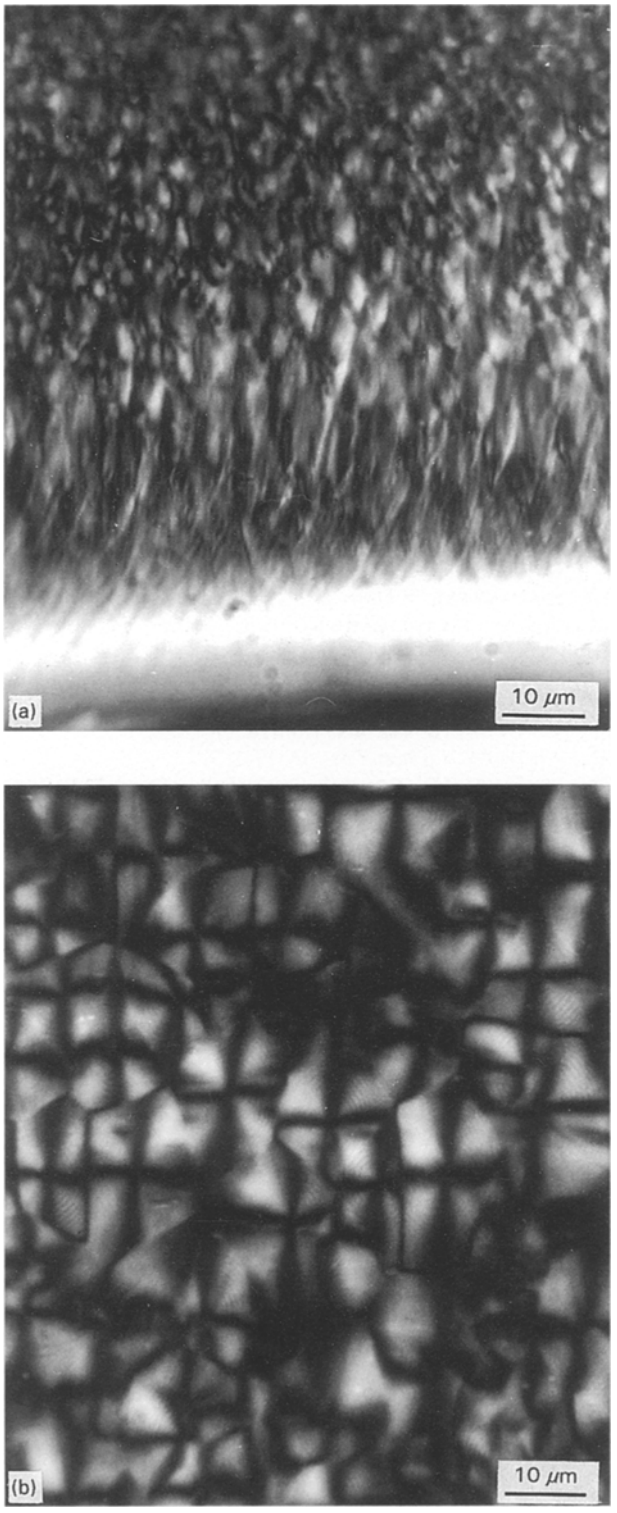

Figure 13 Ringed morphologies: (a) tear-drop and shear zones near the surface; (b) spherulites in the mid-core.

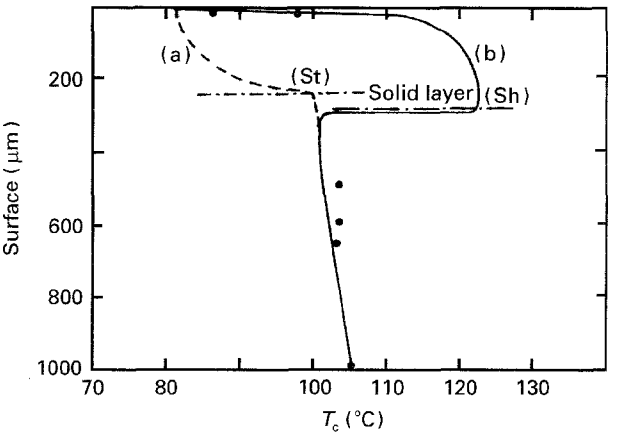

Figure 14 Crystallization temperature inside the thickness of the disc (●) from morphological measurements: (a) prediction of the model without shear effect on the crystallization kinetics (St) (----), (b) prediction of the model with a shear effect on the crystallization kinetics (Sh) (——).

more precisely analysed to show the morphologies and to measure their inner ring spacing. The morphologies in the main part of the shear zone are difficult to analyse. Rings are observed in tear-drop shaped morphologies, very near the surface (Fig. 13a), and in the spherulites crystallized in the central core (Fig. 13b), during the packing–cooling stage. As previously described, the ring spacing is measured only on cut morphologies which include their nuclei. The spacing is larger in tear-drop shaped morphologies than in spherulites. In each position the spacing is measured and the local crystallization temperature is then deduced from Fig. 12 (see Fig. 14).

In the zone crystallized under flow, the crystallization temperature, deduced from ring spacing, strongly increases with the distance from the mould surface. In some locations this temperature is higher than the crystallization temperature in the core zone (Fig. 14). The same figure can be used to compare the crystallization temperature observed in the thickness to those predicted by the thermomechanical model including crystallization models (Sh) and (St). The crystallization temperatures observed and calculated by the thermo-mechanical model, with the two crystallization models, are the same in the core zone. The results are almost identical as an effect of a quasi-static crystallization in this region of the material, which validates the prediction of the model under static conditions. The crystallization temperatures in the shear zone, crystallized during the filling stage, are different. In the zone crystallized under flow, the crystallization model (St) predicts a monotonic increase of the crystallization temperature from the surface to the centre of the core, because the cooling rate, inducing the crystallization, must decrease from the surface to the central part of the thickness. In this zone, the crystallization model with shear effect (Sh) predicts the strong increase of the crystallization temperature with the thickness, observed near the surface in the shear zone. Consequently, the shear flow increases crystallization kinetics, and therefore the thickness of the solid layer and the crystallization temperature up to 25° C. This model also predicts the high crystallization temperature deduced from ring spacing in the shear zone. This temperature is higher than in the core zone, crystallized under quasi-static conditions.

4. Conclusion

Crystallization under shear of a polyethylene was studied, firstly, in order to analyse nucleation and growth mechanisms and, secondly, to check the importance of this kinetics change on polymer solidification during the injection moulding process.

Shear applied during crystallization in isothermal conditions induces row nucleation, increases the growth rate and promotes growth anisotropy of polyethylene. Row nucleation with an unusual direction is observed at the beginning of crystallization under shear and changes in orientation during the experiment. Anisotropic growth is defined by three main growth rates with respect to the main directions of shear experiment. The anisotropy of growth can be explained by an effect of chain orientation with respect to the growth front of lamellae, taking into account the local flow. On the other hand the increase of growth is interpreted by an increase of the equilibrium melting temperature coming from an entropy loss resulting from the chain orientation. These new results mainly come from the direct observation of morphology under a microscope while most of the previous experiments only gave the overall kinetics.

From these data, an overall kinetics equation, with shear effect under constant cooling rate, is proposed as a perturbation of Ozawa's kinetic model. An overall kinetics law was included in a thermo-mechanical model of injection moulding in order to predict polyethylene crystallization. Two thermal kinetics were tested, with and without a shear component. The comparison with experiments shows that a kinetic law with a shear effect is necessary to predict the crystallization temperature and the polymer thickness solidified during the filling stage of the injection moulding process.

References

1. M. D. WOLKOWICZ, J. Polym. Sci. Polym. Symp. **63** (1978) 365.
2. R. R. LAGASSE and B. MAXWELL, *Polym. Eng. Sci.* **16** (1976) 189.
3. C. H. SHERWOOD, F. P. PRICE and R. S. STEIN, *J. Polym. Sci. Polym. Symp.* **63** (1978) 77.
4. M. C. CHIEN and R. A. WEISS, *Polym. Eng. Sci.* **28(1)** (1988) 6.
5. D. L. KRUEGER and G. S. Y. YEH, *J. Appl. Phys.* **43** (1972) 4339.
6. V. TAN and C. G. GOGOS, *Polym. Eng. Sci.* **16** (1976) 512.
7. A. K. FRITZSCHE, F. P. PRICE and R. D. ULRICH, *ibid.* **(3) 16** (1976) 182.
8. P. G. ANDERSEN and S. H. CARR, *ibid.* **18** (1978) 215.
9. K. KOBAYASHI and T. NAGASAWA, *J. Macromol. Sci. Phys.* **B4** (1970) 331.
10. E. S. HSIUE, R. E. ROBERTSON and G. S. Y. YEH, *Polym. Eng. Sci.* **23** (1983) 74.
11. R. D. ULRICH and F. P. PRICE, *J. Appl. Polym. Sci.* **20** (1976) 1095.
12. E. P. CHANG and B. KUSHNER, *Polym. Eng. Sci.* **19** (1979) 1170.
13. A. K. FRITZSCHE and F. P. PRICE, *ibid.* **14** (1974) 401.
14. R. D. ULRICH and F. P. PRICE, *J. Appl. Polym. Sci.* **20** (1976) 1077.
15. W. GEORGE and P. TUCKER, *Polym. Eng. Sci.* **16** (1976) 212.
16. C. DUFOSSÉ, Doctorat thesis, Ecole des Mines de Paris (1990).
17. B. MONASSE, *J. Mater. Sci.* **27** (1992) 6047.
18. G. S. Y. YEH and . Z. HONG, *Polym. Eng. Sci.* **19** (1979) 395.
19. A. J. McHUGH, *J. Appl. Polym. Sci.* **125** (1975) 19.
20. D. ACIERNO, F. P. LA MANTIA and G. MARRUCCI, *Polym. Eng. Sci.* **18** (1978) 817.
21. A. PETERLIN, *ibid.* **16** (1976) 126.
22. P. FLORY, *J. Chem. Phys.* **15** (1947) 397.
23. M. G. BROADHURST, *J. Res. Nat. Bur. Stand.* **70A** (1966) 481.
24. G. S. Y. YEH, K. Z. HONG and D. L. KRUEGER, *Polym. Eng. Sci.* **19** (1979) 401.
25. T. OZAWA, *Polymer* **12** (1971) 150.
26. T. KAWAI, M. IGUCHI and H. TONAMI, *Koll. Z. Z. Polym.* **221** (1967) 28.
27. C. DUFOSSÉ, D. LALART, C. TOURNAIRE, J. M. HAUDIN and B. MONASSE, Crystallization and its effects during injection moulding. *Polymer Processing Society, 6th Annual Meeting*, **3** No. 7, Nice (April, 1990).
28. J. M. HAUDIN and N. BILLON, *Prog. Coll. Polym. Sci.* **87** (1992) 132.

Received 24 March 1994
and accepted 5 April 1995